

Voxel-MAE: Masked Autoencoders for Pre-training Large-scale Point Clouds

Chen Min, Xinli Xu, Dawei Zhao, Liang Xiao, Yiming Nie and Bin Dai

minchen@stu.pku.edu.cn

Abstract

Mask-based pre-training has achieved great success for self-supervised learning in images and languages without manually annotated supervision. However, it has not yet been studied for large-scale point clouds with redundant spatial information. In this research, we propose a mask voxel autoencoder network for pre-training large-scale point clouds, dubbed Voxel-MAE. Our key idea is to transform the point clouds into voxel representations and classify whether the voxel contains point clouds. This simple but effective strategy makes the network voxel-aware of the object shape, thus improving the performance of downstream tasks, such as 3D object detection. Our Voxel-MAE, with even a 90% masking ratio, can still learn representative features for the high spatial redundancy of large-scale point clouds. We also validate the effectiveness of Voxel-MAE on unsupervised domain adaptative tasks, which proves the generalization ability of Voxel-MAE. Our Voxel-MAE proves that it is feasible to pre-train large-scale point clouds without data annotations to enhance the perception ability of the autonomous vehicle. Extensive experiments show great effectiveness of our pre-training method with 3D object detectors (SECOND, CenterPoint, and PV-RCNN) on three popular datasets (KITTI, Waymo, and nuScenes). Codes are publicly available at <https://github.com/chaytonmin/Voxel-MAE>.

1. Introduction

3D object detection aims to obtain accurate 3D information by multiple sensors, which is one of the core techniques in autonomous driving. With the development of deep learning, many datasets containing large-scale point clouds [6, 19, 1] have been published and have extensively promoted the environment perception capability for unmanned vehicles. However, the existing 3D object detection methods rely on large-scale annotated point clouds for model training. Collecting and annotating the datasets consume a lot of money and energy. How to design the self-supervised learning task with the available large amount of unannotated point clouds is of great significance to the per-

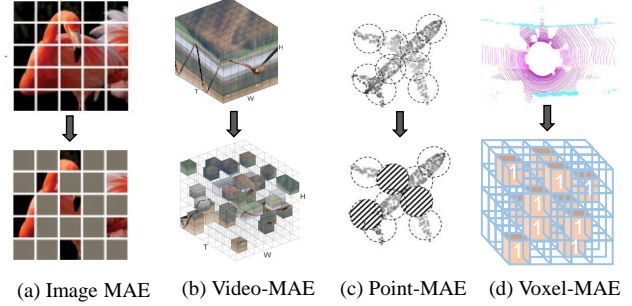


Figure 1. Masked Autoencoders for image [9] (a), video [21] (b), (c) synthetic point clouds [13] (d) and large-scale point clouds of our Voxel-MAE.

ceptual ability of autonomous driving.

Self-supervised learning has been proven to be effective for learning representative features in 2D images [9], videos [5, 21] and synthetic point clouds [13], as shown in Figure 1. However, there is very little research about self-supervised learning for large-scale point clouds. In particular, the simple masked autoencoders (MAE) [9] have been proved effective in learning representative features with the masked data reconstruction task. Similar to 2D images and videos, the large-scale point clouds are also information redundant data, thus designing the MAE for pre-training point clouds is also feasible. However, the large amounts of point clouds in autonomous driving are hard to be reconstructed with neural networks.

In this research, we focus on the voxel representation of large-scale point clouds. The voxel representation is widely used in 3D object detection [32, 25, 16]. Reconstructing the voxel features since a regression task is very difficult as the pre-training network needs to learn the distribution of each point cloud. However, whether the voxel contains point clouds is more important to 3D object detectors. Thus, unlike the pixel reconstruction task in MAE for 2D images, we design the masked voxel classification task for large-scale point clouds, called Voxel-MAE, as illustrated in Fig. 2. That is, we first randomly mask some voxels, then put the unmasked voxels into the 3D encoder built by 3D Spatially Sparse Convolutions [25] and the output of the 3D decoder built by 3D Deconvolutions is the probability of containing

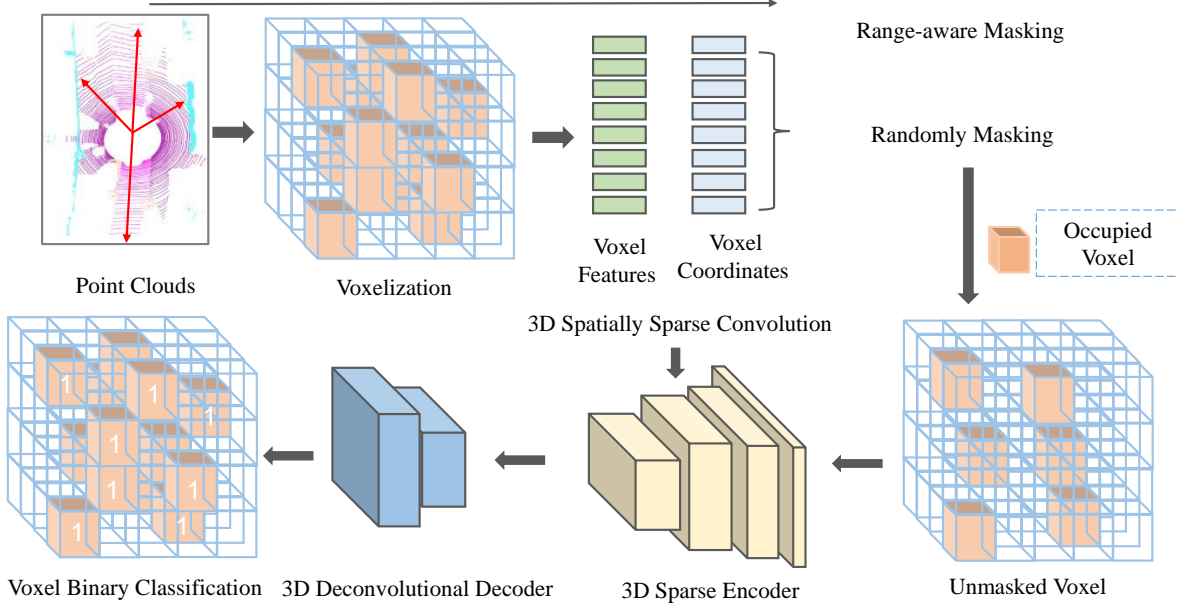


Figure 2. The overall architecture of our Voxel-MAE. We first transform the large-scale irregular point clouds into volumetric representations, and then mask the voxels with the range-aware masking strategy and send the unmasked voxels to the asymmetric encoder-decoder network to reconstruct the voxels. At last, the voxel binary classification loss is used to train the network end to end. Unlike MAE [9], the reconstruction target for large-scale point clouds is set to whether the voxel contains the point clouds, and the Encoder is built with the 3D Spatially Sparse Convolutions to handle the large-scale unmasked voxels.

point clouds for each voxel, at last, we calculate the binary classification loss for the pre-training network. This masked voxel classification task pushes the encoder network voxel-aware of the whole shape of objects, thus learning representative features for 3D object detection. It is worth noting that our Voxel-MAE applies the 3D Spatially Sparse Convolutions to aggregate information from the unmasked data as the Transformers used in MAE [9] can not handle the large-scale unmasked voxels. Besides, we design a range-aware masking strategy considering the sparsity levels of the 3D point clouds at different distances.

We validate the effectiveness of our Voxel-MAE with popular 3D object detectors, such as SECOND [25], CenterPoint [29], and PV-RCNN [16] on three widely used autonomous driving datasets, KITTI [6], Waymo [19] and nuScenes [1]. As most point clouds in autonomous driving are information redundant, Voxel-MAE with even a 90% masking ratio can still learn representative features and improve the performance of 3D object detection. We also validate the effectiveness of Voxel-MAE on unsupervised domain adaptive 3D object detection, which proves the generalization ability of our Voxel-MAE in representation learning.

The main contributions of this work are listed below:

- We propose a novel scheme of masked autoencoders for large-scale point clouds self-supervised learning, namely Voxel-MAE. Unlike the regression task in

MAE, we design the voxel binary classification task for pre-training large-scale point clouds.

- We verify our Voxel-MAE on KITTI, Waymo, and nuScenes datasets with comprehensive experiments. Voxel-MAE effectively improves the performance of 3D object detection methods, such as SECOND, PV-RCNN, and CenterPoint.
- We validate the generalization ability of Voxel-MAE on unsupervised domain adaptive 3D object detection to address the domain shifts in LiDAR-based methods.

2. Related Work

2.1. LiDAR-based 3D Object Detection

LiDAR-based 3D object detection methods with accurate 3D spatial information have been widely used in the field of autonomous driving. Depending on the processing manner for point clouds, these methods can be categorized into point-based, voxel-based, and point-voxel-based.

Point-based object detectors, such as PointRCNN [18] and 3DSSD [28], extract discriminative features from raw point clouds with PointNet [14] and generate proposals centered at each point with 3D region proposal network. The drawback of point-based object detectors is the demand for the high computation cost. To address this problem, voxel-based detectors [32, 25] transform the irregular point clouds

Input	Layer Description	Output	Output Size
Input point clouds	Mean operator	Voxel representation	$1600 \times 1408 \times 41 \times 4$
3D Encoder			
Masked voxels \mathbf{V}_{input}	3DSparseCvonn, filter=(3,3,3), stride=(1,1,1)	Spconv_tensor_1	$1600 \times 1408 \times 41 \times 16$
Spconv_tensor_1	3DSparseCvonn, filter=(3,3,3), stride=(2,2,2)	Spconv_tensor_2	$800 \times 704 \times 21 \times 32$
Spconv_tensor_2	3DSparseCvonn, filter=(3,3,3), stride=(2,2,2)	Spconv_tensor_3	$400 \times 352 \times 11 \times 64$
Spconv_tensor_3	3DSparseCvonn, filter=(3,3,3), stride=(2,2,2)	Spconv_tensor_4	$200 \times 176 \times 5 \times 64$
Spconv_tensor_4	3DSparseCvonn, filter=(1,1,3), stride=(1,1,2)	Latent feature tensor	$200 \times 176 \times 2 \times 128$
3D Decoder			
Latent feature tensor	3DTransCvonn, filter=(3,3,3), stride=(2,2,2)	Dense_tensor_1	$400 \times 354 \times 4 \times 32$
Dense_tensor_1	3DTransCvonn, filter=(3,3,3), stride=(2,2,4)	Dense_tensor_2	$800 \times 704 \times 14 \times 8$
Dense_tensor_2	3DTransCvonn, filter=(3,3,3), stride=(2,2,3)	Occupied voxels \mathbf{P}	$1600 \times 1408 \times 41 \times 1$

Table 1. The details of our Voxel-MAE architecture which consists of a 3D Encoder and a 3D Decoder. 3DSparseCvonn and 3DTransCvonn denote 3D Sparse Convolution proposed in SECOND [25] and common 3D Deconvolution respectively. Here we display the output size for pre-training SECOND on KITTI dataset.

into volumetric representations. The pioneer VoxelNet [32] and its follower SECOND [25] apply the Sparse 3D CNNs to regularize the 4D voxels. PointPillars[10] takes advantage of a standard 2D convolutional detection pipeline that codes point clouds into a special partition of voxels (i.e., pillars) in the light of the tradeoff between efficiency and accuracy. However, the step of point clouds discretization in voxel-based detectors will degrade the fine-grained localization accuracy. Some point-voxel-based methods [16, 3] have been proposed, which take advantage of the localization accuracy of point-based detectors and computational efficiency of voxel-based detectors. PV-RCNN [16] first utilizes 3D sparse CNNs to encode the whole scene and then aggregates the multi-scale semantic voxel-wise features from 3D CNNs into keypoint features for localization refinement. How to design the pre-training network to improve the 3D detection performance has rarely been studied.

2.2. Domain Adaptative 3D Object Detection

Recently, some works have proposed that address the domain shift on point clouds in the 3D object detection task. SN [22] utilizes the target object size distribution before normalizing the object from the source domain to close the size-level domain gap. The source-free domain adaptation method SF-UDA^{3D}[15], first scales the input target sequence data and re-scales the predictions, then uses the time consistency to score and refine the pseudo labels. SR-DAN [31] adopts the scale-aware and range-aware feature adversarial alignment manners to match the distribution between source and target domain. MLC-Net [12] leverages the mean-teacher paradigm with three levels of consistency

to facilitate the cross-domain transfer. The self-denoising frameworks, ST3D [27] and ST3D++ [26], employ three strategies (i.e., random object scaling, hybrid quality-aware triplet memory, and curriculum data augmentation), to reduce noise in pseudo label generation. Though achieving promising results, most of the aforementioned domain adaptation methods ignore the target data distribution when training the model with source data.

2.3. Self-supervised Learning

Self-supervised Learning (SSL) has been popular in recent years without the expensive data annotation. By designing pretext tasks, SSL can learn semantic representations and generalizes well in downstream tasks. [4] first proposes the pretext of predicting the relative location of image patches. Methods in [7, 24, 23] design the pretext task of rotation prediction that has shown promising results in representative feature learning. In [2], a jigsaw puzzle prediction task is proposed and generalizes well in domain adaptation object recognition. Although achieving remarkable progress, the above methods rely on the pretext task of data augmentation. Recently, MAE [9] first masks random patches of the input image and reconstructs the missing pixels with the simple autoencoder framework, showing promising results in self-supervised learning. Video-MAE [21] and method in [5] extend the MAE into spatiotemporal representation learning from videos that are more information redundant. Point-BERT [30] first introduces MAE to pre-train small-scale point clouds. Point-MAE [13] reconstructs the point patches with the Chamfer distance. MaskPoint [11] designs the decoder for discrimi-

nating the masked point patches. In this paper, we explore the effectiveness of masked autoencoders in pre-training the large-scale point clouds, as they are also information redundant.

3. Methodology

Inspired by the great self-supervised learning performance of MAE [9] in 2D images, we design the pre-training network of masked autoencoders for LiDAR-based 3D object detectors to learn representative features. With the n_s unlabeled point cloud data $\{\mathbf{X}^i\}_{i=1}^{n_s}$, we aim to first pre-train the masked autoencoders network ϕ_{pre} with only the point clouds data $\{\mathbf{X}^i\}_{i=1}^{n_s}$ to learn the high-level semantics. Then we use the pre-trained model ϕ_{pre} to warm up the 3D object detection network ϕ_s to improve the detection performance. We also use the pre-trained network model ϕ_{pre} to domain adaptative task for the target point clouds $\{\mathbf{X}^j\}_{j=1}^{n_t}$. The proposed method is shown in Figure 2.

3.1. Masked Autoencoders

Given the instances from large-scale point clouds, the self-supervised pre-training task is to train the network with only the unlabeled data to generate good representations. Developing the proper pretext task is the primary concern in self-supervised learning. The point clouds for 3D object detection in autonomous driving are huge and the masked reconstruction task is unsuitable for large-scale point clouds. To mitigate the issue, we design the pretext task of masked voxel classification task for 3D object detection. We randomly mask the voxels built from the input point clouds and then reconstruct the occupancy voxels with an autoencoder network. The pretext task is trained with the cross-entropy loss. The detailed architecture of Voxel-MAE is demonstrated in Table 1.

3.1.1 Range-aware Masking

Following the typical 3D point cloud detection setting, the point clouds are divided into equally spaced voxels. For the point clouds with range $W \times H \times D$ along the $X \times Y \times Z$ respectively, the size of a voxel is $v_W \times v_H \times v_D$ accordingly. The total number of voxels is n_l , and the number of voxels that contains point clouds is n_v . Following the 3D object detector benchmark SECOND [25], we directly calculate the mean of point features with the 3D coordinates and reflectance intensities in a certain voxel as the voxel-wise representation.

As the large-scale point clouds are information-redundant similar to 2D images, the masking strategy is also suitable for 3D point clouds. However, the 3D point clouds are different from the 2D image as the sparsity levels of the

3D point clouds are correlated to their distances to the LiDAR sensor. The point clouds near the LiDAR sensor are pretty dense, while the point clouds in the far distance are very sparse. Thus we can not perform the same strategy for both the near-range and far-range objects. We should mask a small percentage of point clouds for the far-range objects.

To this end, we use distance information to design the Range-aware Masking strategy, namely, the masking ratio will reduce as the distance to the LiDAR sensor rises. According to the distances to the LiDAR sensor, the voxels that contain point clouds are divided into three groups: 0 - 30m, 30 - 50m, and > 50m, and the corresponding numbers of voxels are n_{v1} , n_{v2} , and n_{v3} . We take the random masking strategy for each group with the descending masking ratio $r1$, $r2$, and $r3$ (i.e., $r1 > r2 > r3$). Thus the number of unmasked occupied voxels is $n_{un} = n_{v1}(1 - r1) + n_{v2}(1 - r2) + n_{v3}(1 - r3)$, and the set of voxels $\mathbf{V}_{input} \in R^{n_{un} \times 4}$ is used as the training set. The occupied voxels containing point clouds (the value of each voxel is 1) and the empty voxels (the value of each voxel is 0) are used as ground truth $\mathbf{T} \in R^{n_l \times 1}$ for voxel classification loss.

3.1.2 3D Sparse Convolutional Encoder

In MAE [9], the Transformer network is selected to perform self-attention on the unmasked portions of the training data, which are not influenced by the masked portions. For 3D point clouds, the number of unmasked voxels is still huge. The Transformer network used in MAE [9] can not aggregate information from all the unmasked input data. In the field of processing large-scale point clouds, the 3D Sparse Convolution [8, 25] is proposed, in which the positional encoding is applied to only aggregate the information from voxels containing point clouds. With the remarkable efficiency of 3D Sparse Convolution, many popular 3D object detection methods [25, 16, 29, 28] have been proposed. Inspired by this, we adopt the 3D Spatially Sparse Convolution proposed in SECOND [25] to build the encoder network to aggregate information from only the unmasked voxels that contain point clouds with the positional encoding module, thus our voxel masking strategy can reduce the memory complexity for training, similar to Transformer network in MAE [9].

3.1.3 3D Deconvolutional Decoder

Our decoder consists of several 3D Convolution layers, and the last layer outputs the probability that each voxel contains point clouds. The output of decoder is $\mathbf{P} \in R^{n_l \times 1}$. The decoder is only used during pre-training to perform the voxel reconstruction task. Shifting mask tokens to the decoder can make the encoder learn better latent features for downstream tasks.

Table 2. Performance comparison on the KITTI *val* split with AP calculated by 11 recall positions.

Method	Car	Pedestrian	Cyclist
SECOND [25]	78.62	52.98	67.15
Voxel-MAE + SECOND	78.90	53.14	68.08
SECOND-IOU [27]	79.09	55.74	71.31
Voxel-MAE + SECOND-IOU	79.22	55.79	72.22
PV-RCNN [16]	83.61	57.90	70.47
Voxel-MAE + PV-RCNN	83.82	59.37	71.99

3.1.4 Reconstruction Target

In MAE [9], the goal is to reconstruct the RGB pixel values in the masked patches as a regression task. However, regression of the voxel features is challenging as the network needs to learn the distribution of each point cloud. For the 3D point cloud detectors, the model is more sensitive to whether the voxel contains point clouds. Inspired by this, we design the voxel classification task for large-scale point clouds pre-training. We use the 3D Convolutional layer as the prediction head to produce the reconstructed occupied voxels. The aim is to recover the coordinates of voxels in the masked set. Given the predicted occupied voxels \mathbf{P} and ground truth occupied voxels \mathbf{T} , we calculate the binary voxel classification loss of cross-entropy:

$$loss = -\frac{1}{batch} \sum_{i=1}^{batch} \sum_{j=1}^{n_i} \mathbf{T}_j^i \log \mathbf{P}_j^i, \quad (1)$$

where \mathbf{P}_j^i is the predicted probability of voxel j of the i -th training sample, and \mathbf{T}_j^i is the corresponding ground truth whether the voxel contains point clouds.

Albeit simple, the masked voxel classification loss effectively introduces the information of point cloud non-uniform distribution to facilitate the network to learn representative features.

4. Experiments

4.1. Experimental Setup

Dataset The three popular autonomous driving datasets: KITTI [6], Waymo [19], and nuScenes [1] are used in our experiments.

KITTI. The KITTI dataset [6] is one of the most popular autonomous driving datasets, which provides 7,481 training samples and 7,518 testing samples. The 3D bounding box annotations are only provided within the Field of View (FoV) of the front camera. We follow the common 50/50 *train/val* split and use the official KITTI evaluation metrics for three-level evaluation (Easy, Moderate, Hard) and the mean average precision is evaluated.

Waymo Open Dataset. The Waymo Open Dataset [19] is a recently released large-scale autonomous driving

dataset, which consists of total 798 training sequences with around 158,361 LiDAR samples, and 202 validation sequences with 40,077 LiDAR samples. Following the popular point cloud detection codebase OpenPCDet [20], we subsample a single frame of 20% data (about 32k frames) of all the training samples as the training set. It annotated the objects in the full 360° field. The official evaluation metrics of Waymo are mean average precision (AP) and mean average precision weighted by heading (APH) in difficulty levels (L1 and L2).

nuScenes. The nuScenes dataset [1] is another popular autonomous driving dataset. There are total 28,130 training samples and 6,019 validation samples. We evaluate with the official evaluation metrics of the nuScenes Detection Score (NDS), mean average precision (mAP), average translation error (ATE), average scale error (ASE), average orientation error (AOE), average velocity error (AVE), average attribute error (AAE).

Implementation Details We adopt the training settings of the popular point clouds detection codebase OpenPCDet [20] (version 0.5.2). For KITTI dataset, the detection range is set to [0, 70.4m] for X axes, [-40m, 40m] for Y axes, [-3m, 1m] for Z axes, and the voxel size is set to (0.05m, 0.05m, 0.1m). For the Waymo dataset, the detection range is set to [-75.2m, 75.2m] for X and Y axes, [-2m, 4m] for Z axes, and the voxel size is set to (0.1m, 0.1m, 0.15m). For nuScenes dataset, the detection range is set to [-51.2m, 51.2m] for X and Y axes, [-5m, 3m] for Z axes, and the voxel size is set to (0.1m, 0.1m, 0.2m). The masking ratios for voxels in 0 - 30m, 30 - 50m, and > 50m are set as 90%, 70%, and 50% for three datasets. The number of pre-training epochs is set as 3 for three datasets.

Following OpenPCDet, we use the common augmentations, including random world flipping and random world scaling in training Voxel-MAE. The ADAM optimizer and cosine annealing learning rate strategy are adopted. More detailed parameter setups could be found in OpenPCDet.

4.2. Results and Analysis

Table 2 shows the performance of the proposed pre-training network Voxel-MAE on KITTI *val* set. Although the number of samples in KITTI is small, our Voxel-MAE can still improve SECOND [25] and PV-RCNN [16], especially for small objects (i.e., pedestrian and cyclist). We also find that our Voxel-MAE can improve the evaluation of the bounding box and orientation a lot, as shown in Table 3. We ascribe this performance gain to our voxel masking strategy, which helps to learn high-level semantic information as the Voxel-MAE needs to recover these missing voxels. The bounding box and orientation prediction will benefit from such a design.

To further validate the effectiveness of our proposed

Table 3. Performance comparison on the KITTI *val* split with AP calculated by 11 recall positions evaluating bounding box and orientation.

Evaluation	Method	Car			Pedestrian			Cyclist		
		Easy	Moderate	Hard	Easy	Moderate	Hard	Easy	Moderate	Hard
bbox	SECOND [25]	90.73	89.76	88.94	68.70	65.27	62.52	87.88	75.43	71.67
	Voxel-MAE + SECOND	94.81	89.98	89.35	70.37	67.45	65.14	91.82	78.65	73.77
aos	SECOND [25]	90.73	89.63	88.70	63.46	60.13	56.93	87.63	74.67	71.00
	Voxel-MAE + SECOND	94.66	89.88	88.92	65.33	61.55	59.23	91.57	78.42	73.50

Table 4. Quantitative detection performance achieved by different methods on the Waymo *val* set.

Method	Vec.L1		Vec.L2		Ped.L1		Ped.L2		Cyc.L1		Cyc.L2	
	mAP	mAPH	mAP	mAPH	mAP	mAPH	mAP	mAPH	mAP	mAPH	mAP	mAPH
SECOND [25]	70.96	70.34	62.58	62.02	65.23	54.24	57.22	47.49	57.13	55.62	54.97	53.53
Voxel-MAE + SECOND	71.12	70.58	62.67	62.34	67.21	55.68	59.03	48.79	57.73	56.18	55.62	54.17
CenterPoint [29]	71.33	70.76	63.16	62.65	72.09	65.49	64.27	58.23	68.68	67.39	66.11	64.87
Voxel-MAE + CenterPoint	71.89	71.33	64.05	63.53	73.85	67.12	65.78	59.62	70.29	69.03	67.76	66.53
PV-RCNN(Anchor) [16]	75.41	74.74	67.44	66.80	71.98	61.24	63.70	53.95	65.88	64.25	63.39	61.82
Voxel-MAE + PV-RCNN(Anchor)	75.94	75.28	67.94	67.34	74.02	63.48	64.91	55.57	67.21	65.49	64.62	63.02
PV-RCNN(Center) [20]	75.95	75.43	68.02	67.54	75.94	69.40	67.66	61.62	70.18	68.98	67.73	66.57
Voxel-MAE + PV-RCNN(Center)	77.29	76.81	68.71	68.21	77.70	71.13	69.53	63.46	70.55	69.39	68.11	66.95
PV-RCNN++ [17]	77.82	77.32	69.07	68.62	77.99	71.36	69.92	63.74	71.80	70.71	69.31	68.26
Voxel-MAE + PV-RCNN++	78.23	77.72	69.54	69.12	79.85	73.23	71.07	64.96	71.75	70.64	69.26	68.21

Voxel-MAE, we evaluate the performance of Voxel-MAE on the large-scale Waymo and nuScenes datasets. Table 4 shows that our method improves the popular 3D point cloud detection methods SECOND [25], CenterPoint [29], and PV-RCNN [16] in terms of mAP and mAPH. Voxel-MAE also improves 3D detection performance on nuScenes in Table 5. The experimental results on the large-scale Waymo and nuScenes dataset further validate the great representative features obtained by our simple Voxel-MAE on various datasets. Results for SECOND [25], CenterPoint [29], and PV-RCNN [16] are from OpenPCDet [20].

4.3. Unsupervised Domain Adaptation

The domain shifts in LiDAR-based 3D objectors are apparent as the LiDARs have different scan patterns. Evaluation of datasets captured in different locations, conditions, or sensors than that of the training (source) data results in a drop in model performance due to the gap in distribution with the test (or target) data. To further investigate the generalization ability of Voxel-MAE in representation learning, we conduct experiments in two scenarios of unsupervised domain adaptative (UDA) 3D object detection: different data collection locations and time (i.e., Waymo \rightarrow KITTI) and different LiDAR ring numbers (i.e., nuScenes \rightarrow KITTI). We compare our method with (1) Oracle, where the model training and evaluation are both on the target domain; (2) Source-only, where the pre-trained model is directly used on the target domain inferring; (3) SN [22], a weakly-supervised domain adaptation method with the statistical information of target domain object size;

(4) ST3D [27], the SOTA UDA 3D object detection method with self-training strategy and (5) ST3D(w/SN) [27], where the weakly-supervised DA setting utilizes the target object size distribution as prior. We follow the setting in the recently published UDA method ST3D [27] and use the pre-trained model by our Voxel-MAE on both the source and target data to train ST3D. From Table 6, we can see that with our Voxel-MAE, the performance of UDA is improved, demonstrating that our Voxel-MAE can learn more transferable representations.

4.4. Ablation Studies

In this section, we conduct extensive ablation experiments to investigate the individual components of our Voxel-MAE. All experiments are conducted with the 3D object detector SECOND [25] on KITTI *val* split.

4.4.1 Pretext Task

We now analyze the influence of the reconstruction task of Voxel-MAE. In Table 7 we can observe that the results of the voxel regression task will decrease. This is because the voxel classification task is easier for the network to learn and whether the voxel contains point clouds is more critical for voxel-based 3D object detection methods. With the simple voxel binary classification task, the pre-trained network would be voxel-aware of object shape, thus improving the performance of the downstream tasks. The results in Table 7 are achieved by 11 recall positions evaluating 3d detection in three categories.

Table 5. Quantitative detection performance achieved by different methods on the nuScenes *val* set.

Method	mAP \uparrow	NDS \uparrow	mATE \downarrow	mASE \downarrow	mAOE \downarrow	mAVE \downarrow	mAAE \downarrow
SECOND [25]	50.59	62.29	31.15	25.51	26.64	26.26	20.46
Voxel-MAE + SECOND	50.82	62.45	31.02	25.23	26.12	26.11	20.04
CenterPoint [29]	56.03	64.54	30.11	25.55	38.28	21.94	18.87
Voxel-MAE + CenterPoint	56.45	65.02	29.73	25.17	38.38	21.47	18.65

Table 6. Quantitative results of adaptation tasks. Our Voxel-MAE improves the performance of UDA 3D object detection.

Task	Method	PV-RCNN	
		BEV	3D
Waymo \rightarrow KITTI	Oracle	88.98	82.50
	Source-only	61.18	22.01
	SN [22]	79.78	63.60
	ST3D [27]	84.10	64.78
	ST3D(w/SN) [27]	86.65	76.86
	Voxel-MAE + ST3D	85.52	65.24
nuScenes \rightarrow KITTI	Oracle	88.98	82.50
	Source-only	68.15	37.17
	SN [22]	60.48	49.47
	ST3D [27]	78.36	70.85
	ST3D(w/SN) [27]	84.29	72.94
	Voxel-MAE + ST3D	78.66	71.24
	Voxel-MAE + ST3D(w/SN)	85.43	73.22

Table 7. Impacts of pretext task.

Target	Car	Pedestrian	Cyclist
Regression	78.67	52.99	67.32
Classification	78.90	53.14	68.08

Table 8. Impacts of masking ratio.

Masking ratio			Easy	Moderate	Hard
0-30m	30-50m	>50m			
0.3	0.3	0.3	96.96	94.75	93.97
0.5	0.5	0.5	97.03	94.79	94.00
0.7	0.5	0.3	97.16	94.92	94.25
0.7	0.7	0.7	97.14	94.78	94.11
0.9	0.7	0.5	97.12	96.12	94.23
0.9	0.7	0.7	97.11	96.07	94.15
0.9	0.9	0.9	97.00	96.06	94.13

4.4.2 Masking Ratio

In this section, we study the effect of the voxel masking ratio on the pre-training input. It can be seen from Table 8 that an extremely high masking ratio (90%) can still achieve good representations. The small masking ratio for far-range voxels will improve the detection performance. The results

Table 9. Impacts of pre-training times.

Epoch	Easy	Moderate	Hard
1	78.98	66.13	61.55
2	81.26	67.23	61.68
3	82.09	68.05	62.08
4	82.12	68.00	61.99

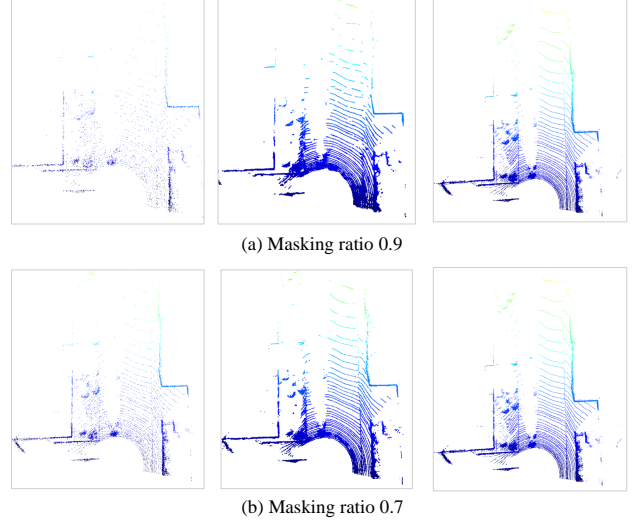


Figure 3. Input unmasked voxels (left), Reconstructed voxels (middle), and Original voxels (right). Masking ratios are 90% and 70%.

in Table 8 are achieved by 40 recall positions evaluating 3d detection in car category with IOU threshold of 0.5.

4.4.3 Pre-training Times

Table 9 shows the influence of the training times. The results are achieved by 11 recall positions evaluating 3d detection in the cyclist category with an IOU threshold of 0.5. With the increment of training times, the performance increases at first and afterward will remain stable.

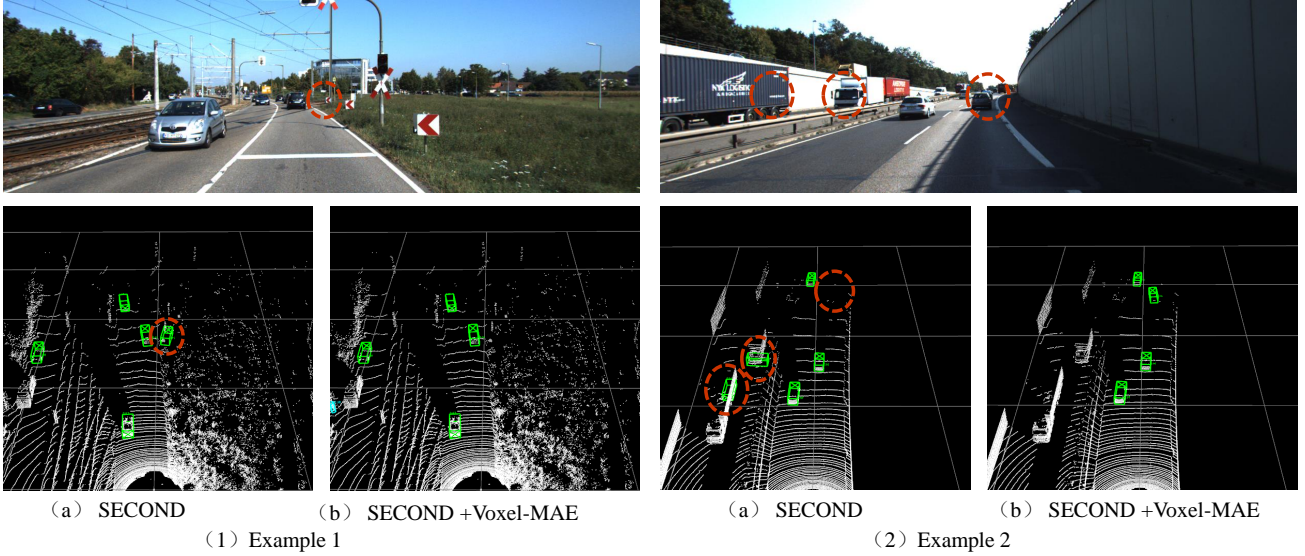


Figure 4. Qualitative results achieved on the KITTI *test* set. With the pre-training of our Voxel-MAE, the 3D detector can learn more robust features to reduce missed and false detection.

4.5. Visualization

We show the reconstructed voxels in Figure 3 with masking ratios of 90% and 70%. The masked voxels are randomly selected from the whole non-empty voxels. We can see that the Voxel-MAE can reconstruct the masked objects well.

Figure 4 shows the visualization of predictions by SECOND [25] and SECOND with pre-training of our Voxel-MAE. The limited resolution of LiDAR will lead to missed and false detection of faraway objects. With our Voxel-MAE, the detectors will learn more robust features to improve detection as shown in Figure 4 (1). Occlusion is another challenging problem in 3D object detection, as shown in Figure 4 (2), the masked voxel classification task pushes Voxel-MAE to be voxel-aware of the whole shape of objects, thus improving the detection for the Occlusion areas.

5. Conclusion

In this paper, we introduce a simple large-scale point clouds self-supervised learning method, named Voxel-MAE. Our Voxel-MAE first randomly masks the input voxels with the range-aware masking strategy and then reconstructs the voxels. Unlike 2D MAE, we design the voxel classification task for large-scale point clouds, which would encourage the Voxel-MAE to reason over high-level semantics to recover these masked voxels, because whether the voxel contains point clouds is very important for 3D object detection. Our extensive experimental results demonstrate the effectiveness of Voxel-MAE on three popular autonomous driving datasets, KITTI, Waymo, and nuScenes. In the future, we are planning to validate the effectiveness of

Voxel-MAE in more downstream tasks for large-scale point clouds.

References

- [1] Holger Caesar, Varun Bankiti, Alex H Lang, Sourabh Vora, Venice Erin Liong, Qiang Xu, Anush Krishnan, Yu Pan, Giancarlo Baldan, and Oscar Beijbom. nuscenes: A multi-modal dataset for autonomous driving. In *Proceedings of the IEEE/CVF conference on computer vision and pattern recognition*, pages 11621–11631, 2020. 1, 2, 5
- [2] Fabio M Carlucci, Antonio D’Innocente, Silvia Bucci, Barbara Caputo, and Tatiana Tommasi. Domain generalization by solving jigsaw puzzles. In *Proceedings of the IEEE/CVF Conference on Computer Vision and Pattern Recognition*, pages 2229–2238, 2019. 3
- [3] Yilun Chen, Shu Liu, Xiaoyong Shen, and Jiaya Jia. Fast point r-cnn. In *Proceedings of the IEEE/CVF international conference on computer vision*, pages 9775–9784, 2019. 3
- [4] Carl Doersch, Abhinav Gupta, and Alexei A Efros. Unsupervised visual representation learning by context prediction. In *Proceedings of the IEEE international conference on computer vision*, pages 1422–1430, 2015. 3
- [5] Christoph Feichtenhofer, Haoqi Fan, Yanghao Li, and Kaiming He. Masked autoencoders as spatiotemporal learners. *arXiv preprint arXiv:2205.09113*, 2022. 1, 3
- [6] Andreas Geiger, Philip Lenz, and Raquel Urtasun. Are we ready for autonomous driving? the kitti vision benchmark suite. In *2012 IEEE conference on computer vision and pattern recognition*, pages 3354–3361. IEEE, 2012. 1, 2, 5
- [7] Spyros Gidaris, Praveer Singh, and Nikos Komodakis. Unsupervised representation learning by predicting image rotations. *arXiv preprint arXiv:1803.07728*, 2018. 3
- [8] Benjamin Graham, Martin Engelcke, and Laurens Van Der Maaten. 3d semantic segmentation with submani-

- fold sparse convolutional networks. In *Proceedings of the IEEE conference on computer vision and pattern recognition*, pages 9224–9232, 2018. 4
- [9] Kaiming He, Xinlei Chen, Saining Xie, Yanghao Li, Piotr Dollár, and Ross Girshick. Masked autoencoders are scalable vision learners. In *Proceedings of the IEEE/CVF Conference on Computer Vision and Pattern Recognition*, pages 16000–16009, 2022. 1, 2, 3, 4, 5
- [10] Alex H Lang, Sourabh Vora, Holger Caesar, Lubing Zhou, Jiong Yang, and Oscar Beijbom. Pointpillars: Fast encoders for object detection from point clouds. In *Proceedings of the IEEE/CVF conference on computer vision and pattern recognition*, pages 12697–12705, 2019. 3
- [11] Haotian Liu, Mu Cai, and Yong Jae Lee. Masked discrimination for self-supervised learning on point clouds. *arXiv preprint arXiv:2203.11183*, 2022. 3
- [12] Zhipeng Luo, Zhongang Cai, Changqing Zhou, Gongjie Zhang, Haiyu Zhao, Shuai Yi, Shijian Lu, Hongsheng Li, Shanghang Zhang, and Ziwei Liu. Unsupervised domain adaptive 3d detection with multi-level consistency. In *Proceedings of the IEEE/CVF International Conference on Computer Vision*, pages 8866–8875, 2021. 3
- [13] Yatian Pang, Wenxiao Wang, Francis EH Tay, Wei Liu, Yonghong Tian, and Li Yuan. Masked autoencoders for point cloud self-supervised learning. *arXiv preprint arXiv:2203.06604*, 2022. 1, 3
- [14] Charles R Qi, Hao Su, Kaichun Mo, and Leonidas J Guibas. Pointnet: Deep learning on point sets for 3d classification and segmentation. In *Proceedings of the IEEE conference on computer vision and pattern recognition*, pages 652–660, 2017. 2
- [15] Cristiano Saltori, Stéphane Lathuilière, Nicu Sebe, Elisa Ricci, and Fabio Galasso. Sf-uda 3d: Source-free unsupervised domain adaptation for lidar-based 3d object detection. In *2020 International Conference on 3D Vision (3DV)*, pages 771–780. IEEE, 2020. 3
- [16] Shaoshuai Shi, Chaoxu Guo, Li Jiang, Zhe Wang, Jianping Shi, Xiaogang Wang, and Hongsheng Li. Pv-rcnn: Point-voxel feature set abstraction for 3d object detection. In *Proceedings of the IEEE/CVF Conference on Computer Vision and Pattern Recognition*, pages 10529–10538, 2020. 1, 2, 3, 4, 5, 6
- [17] Shaoshuai Shi, Li Jiang, Jiajun Deng, Zhe Wang, Chaoxu Guo, Jianping Shi, Xiaogang Wang, and Hongsheng Li. Pv-rcnn++: Point-voxel feature set abstraction with local vector representation for 3d object detection. *arXiv preprint arXiv:2102.00463*, 2021. 6
- [18] Shaoshuai Shi, Xiaogang Wang, and Hongsheng Li. Point-rcnn: 3d object proposal generation and detection from point cloud. In *Proceedings of the IEEE/CVF conference on computer vision and pattern recognition*, pages 770–779, 2019. 2
- [19] Pei Sun, Henrik Kretschmar, Xerxes Dotiwalla, Aurelien Chouard, Vijaysai Patnaik, Paul Tsui, James Guo, Yin Zhou, Yuning Chai, Benjamin Caine, et al. Scalability in perception for autonomous driving: Waymo open dataset. In *Proceedings of the IEEE/CVF conference on computer vision and pattern recognition*, pages 2446–2454, 2020. 1, 2, 5
- [20] OpenPCDet Development Team. Openpcdet: An open-source toolbox for 3d object detection from point clouds. <https://github.com/open-mmlab/OpenPCDet>, 2020. 5, 6
- [21] Zhan Tong, Yibing Song, Jue Wang, and Limin Wang. Videomae: Masked autoencoders are data-efficient learners for self-supervised video pre-training. *arXiv preprint arXiv:2203.12602*, 2022. 1, 3
- [22] Yan Wang, Xiangyu Chen, Yurong You, Li Erran Li, Bharath Hariharan, Mark Campbell, Kilian Q Weinberger, and Wei-Lun Chao. Train in germany, test in the usa: Making 3d object detectors generalize. In *Proceedings of the IEEE/CVF Conference on Computer Vision and Pattern Recognition*, pages 11713–11723, 2020. 3, 6, 7
- [23] Liang Xiao, Jiaolong Xu, Dawei Zhao, Zhiyu Wang, Li Wang, Yiming Nie, and Bin Dai. Self-supervised domain adaptation with consistency training. In *2020 25th International Conference on Pattern Recognition (ICPR)*, pages 6874–6880. IEEE, 2021. 3
- [24] Jiaolong Xu, Liang Xiao, and Antonio M López. Self-supervised domain adaptation for computer vision tasks. *IEEE Access*, 7:156694–156706, 2019. 3
- [25] Yan Yan, Yuxing Mao, and Bo Li. Second: Sparsely embedded convolutional detection. *Sensors*, 18(10):3337, 2018. 1, 2, 3, 4, 5, 6, 7, 8
- [26] Jihan Yang, Shaoshuai Shi, Zhe Wang, Hongsheng Li, and Xiaojuan Qi. St3d++: Denoised self-training for unsupervised domain adaptation on 3d object detection. *arXiv preprint arXiv:2108.06682*, 2021. 3
- [27] Jihan Yang, Shaoshuai Shi, Zhe Wang, Hongsheng Li, and Xiaojuan Qi. St3d: Self-training for unsupervised domain adaptation on 3d object detection. In *Proceedings of the IEEE/CVF Conference on Computer Vision and Pattern Recognition*, pages 10368–10378, 2021. 3, 5, 6, 7
- [28] Zetong Yang, Yanan Sun, Shu Liu, and Jiaya Jia. 3dssd: Point-based 3d single stage object detector. In *Proceedings of the IEEE/CVF conference on computer vision and pattern recognition*, pages 11040–11048, 2020. 2, 4
- [29] Tianwei Yin, Xingyi Zhou, and Philipp Krahenbuhl. Center-based 3d object detection and tracking. In *Proceedings of the IEEE/CVF conference on computer vision and pattern recognition*, pages 11784–11793, 2021. 2, 4, 6, 7
- [30] Xumin Yu, Lulu Tang, Yongming Rao, Tiejun Huang, Jie Zhou, and Jiwen Lu. Point-bert: Pre-training 3d point cloud transformers with masked point modeling. In *Proceedings of the IEEE/CVF Conference on Computer Vision and Pattern Recognition*, pages 19313–19322, 2022. 3
- [31] Weichen Zhang, Wen Li, and Dong Xu. Srdan: Scale-aware and range-aware domain adaptation network for cross-dataset 3d object detection. In *Proceedings of the IEEE/CVF Conference on Computer Vision and Pattern Recognition*, pages 6769–6779, 2021. 3
- [32] Yin Zhou and Oncel Tuzel. Voxelnet: End-to-end learning for point cloud based 3d object detection. In *Proceedings of the IEEE conference on computer vision and pattern recognition*, pages 4490–4499, 2018. 1, 2, 3